Bioconjugate Chemistry

Article

pubs.acs.org/bc

Monitoring Cellular Uptake and Cytotoxicity of Copper(II) Complex Using a Fluorescent Anthracene Thiosemicarbazone Ligand

Anup N. Kate,[†] Anupa A. Kumbhar,*[,†] Ayesha A. Khan,[†] Pranaya V. Joshi,[‡] and Vedavati G. Puranik[‡]

[†]Department of Chemistry, University of Pune, Pune 411007, India

[‡]Centre for Materials Characterization, National Chemical Laboratory, Pune 411008, India

Supporting Information

ABSTRACT: The thiosemicarbazone derivative of anthracene (ATSC, anthracene thiosemicarbazone **1**) and its copper(II) complex (CuATSC, **2**) were synthesized and characterized by spectroscopic, electrochemical, and crystallographic techniques. Interaction of **1** and **2** with calf thymus (CT) DNA was explored using absorption and emission spectral methods, and viscosity measurements reveal a partial-intercalation binding mode. Their protein binding ability was monitored by the quenching of tryptophan emission using bovine serum albumin (BSA) as a model protein. Furthermore, their cellular uptake, in vitro cytotoxicity testing on the HeLa cell line, and flow cytometric analysis were carried out to ascertain the mode of cell death. Cell cycle analysis indicated that **1** and **2** cause cell cycle arrest in sub-G1 phase.

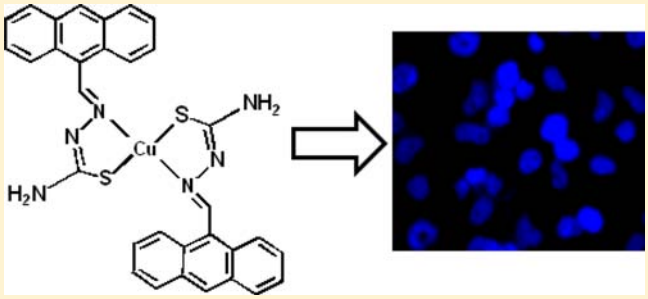

INTRODUCTION

Transition-metal complexes have been extensively studied as anticancer drugs because of their diverse spectral, chemical, and electrochemical properties.[1−9] Cisplatin is the most widely employed metal-based anticancer drug used in the clinic; however, its use is limited because of toxic side effects that limit the dose that can be administered to patients.[9] This has stimulated the search for novel nonplatinum metal species as cytotoxic agents. Thus, in recent years, a large number of nonplatinum transition-metal complexes, especially biocompatible Cu(II) complexes, have been investigated for their biological properties.[10−13]

Thiosemicarbazone derivatives represent a class of organic compounds that have been explored because of their broad spectrum of biological activities.[14−16] It is one of several classes of copper-coordinating lipophilic compounds being investigated as potential anticancer therapeutics, especially for prostate, cervical, ovarian, breast, stomach, and lung cancer, where elevated levels of intracellular copper have been demonstrated.[17−20] Some Cu(II) thiosemicarbazone complexes such as Cu^{II}(ATSM), Cu^{II}(GTSM), and Cu^{II}(PTSM) have been reported to be active as hypoxia-imaging agents.[21] Recently, interest has focused on developing less toxic analogues of these thiosemicarbazones to gain better understanding of their mechanism of action.[22,23] It has been observed that changes in the ligand backbone can significantly alter the biological activity of copper complexes, which is exemplified by Cu^{II}(ATSM) and Cu^{II}(GTSM). Unlike Cu^{II}(ATSM), which has two methyl groups on the diketone backbone, Cu^{II}(GTSM) releases its copper intracellularly under normoxic conditions without reported side effects.[24] It is also being investigated as a therapeutic for Alzheimer's disease,[25] whereas Cu^{II}(ATSM) has shown potential as a drug for Parkinson's disease in animal models.[26] Marisa Belicchi-Ferrari and co-workers have reported pyridoxal thiosemicarbazone copper(II) complexes with nitroprusside as a counterion.[27] These complexes were found to exert antiproliferative activity on the CEM and U937 cell lines, inducing apoptosis. Cytotoxic activity of copper(II) complexes with thiosemicarbazone ligands containing a pyrazolone moiety have been studied by Vukadin Leovac et al. on the HL60, REH, C6, L929, and B16 cell lines.[28]

To be an effective anticancer drug, the metal complex must reach the appropriate target inside the cell. Labeling a ligand with a fluorophore makes the metal complex luminescent. This allows it to be tracked by means of fluorescence microscopy and flow cytometry, which are nondestructive techniques that also permit live cell imaging.[29−34] Donelly and co-workers have recently reported the cell permeability and intracellular distribution of pyrene-appended bis(thiosemicarbazonato) copper(II) complexes using confocal fluorescence microscopy.[35]

In our efforts to synthesize a therapeutic reporter molecule that can be monitored by noninvasive techniques without using radionuclides, we appended thiosemicarbazone with anthracene. Anthracene derivatives are the most important class of ligands with high intrinsic fluorescence; they have been investigated for their binding to DNA, and some are promising chemotherapeutic agents.[36−38] Anthracene itself has been

Received: August 20, 2013
Revised: December 11, 2013
Published: December 11, 2013

dx.doi.org/10.1021/bc400385d | *Bioconjugate Chem.* 2014, 25, 102−114

Table 1. UV−Vis and Emission Data for 1 and 2

compound[a]	absorbance[b], λ_{max} (nm) (ε (M^{-1} cm^{-1}))	emission[b]					
		λ_{em} (nm)	φ_{em}[c]	τ_1 (ns)[c]	τ_2 (ns)[c]	$k_r \times 10^6$	$k_{nr} \times 10^6$
1	310 (11 910), 402 (15 571)	500	0.057	2.05	7.44	6.93	2.82
2	306 (14 500), 400 (16 900), 690 (144)	500	0.044	2.28	9.25	7.44	2.40

[a][1] and [2] = 100 μM. [b]Spectra were recorded in DMSO at 298 K; λ_{ex} = 370 nm. [c]φ_{em} = emission quantum yield, and lifetime measurements were carried out in ethanol solvent. Error limit: λ_{max} = ± 2 nm, λ_{em} = ± 2 nm, and φ_{em} = ±3%

reported to be effective against psoriasis.[39] Other anthracene derivatives tested for their anticancer activity include mitoxantrone, ametantrone, and bisantrene, which have been suggested to elicit their activity by binding to DNA through groove/electrostatic as well as intercalative binding modes.[40−42] The combined effect of thiosemicarbazone pharmacophore with anthracene (ATSC, **1**) and its Cu(II) complex (CuATSC, **2**) was investigated in terms of their DNA and protein-binding ability and DNA-cleavage properties. Their cellular uptake was monitored by fluorescence microscopy, and correlation of their anticancer efficacy on cervical cancer cells (HeLa cells) with their redox potential was made. Cells harvested 24 h after treatment with the compounds were found to be arrested in the S and G2/M phases of the cell cycle, which further progresses into apoptosis.

EXPERIMENTAL PROCEDURES

Materials. All reagents and solvents were purchased commercially and were used as received. Copper(II) chloride dihydrate, thiosemicarbazide, and glacial acetic acid were purchased from SD Fine Chemicals (India); anthraldehyde was purchased from Aldrich. Bovine serum albumin (BSA, fraction V) was purchased from SRL (India); supercoiled plasmid pBR322 DNA was obtained from Chromous Biotech (India).

Synthesis of Anthracene Thiosemicarbazone (ATSC, 1). Anthracene thiosemicarbazone was synthesized as reported previously.[43] Thiosemicarbazide (0.091 g, 1 mmol) and 9-anthraldehyde (0.206 g, 1 mmol) were suspended in ethanol (20 mL) containing a few drops of glacial acetic acid. The mixture was refluxed for 3 h and cooled to room temperature. The orange-yellow product that formed was filtered off, washed with cold ethanol and ether, and dried in vacuo. It was recrystallized from ethanol, giving a yield of 82% (229.1 mg) as an orange-yellow solid. IR (KBr pellet, cm^{-1}): ν 3441, 3045, 3030 (NH_2, NH), 1601 (C═N), 1020 (N−N), 846 (C═S). ^{1}H NMR (300 MHz, DMSO-d_6) 11.66 (1H, s), 9.33 (1H, s), 8.71 (1H, s), 8.55−8.58 (2H, d), 8.17 (1H, s), 8.13−8.15 (2H, d), 7.57−7.59 (4H, m). ESI-MS: m/z $[M + H]^+$ 280. Anal. Calcd for $C_{16}H_{13}N_3S$: C, 68.8; H, 4.7; N, 15.0. Found: C, 68.52; H, 4.7; N, 14.37.

Synthesis of Cu(ATSC)$_2$ (CuATSC, 2). This complex was prepared by addition of an ethanolic solution of ATSC (0.200 g, 0.716 mM) to a solution of copper(II) chloride dihydrate (0.061 g, 0.358 mM) in ethanol, which was then stirred for 3 to 4 h at room temperature. The precipitate that formed was collected by filtration and washed with small amounts of ethanol/acetone followed by diethyl ether and dried in vacuo. Yield: 0.145 g (55.0%). IR (KBr pellet, cm^{-1}): ν 3049, 3001 (NH_2 stretch), 1593 (C═N), 812 (C═S). ESI-MS: m/z $[M + 2\ ACN + MeOH + H]^+$ 736.2. Anal. Calcd for $C_{32}H_{24}N_6S_2Cu$: C, 61.2; H, 3.90; N, 13.54. Found: C, 59.79; H, 3.62; N, 13.48

Physical Measurements. UV−vis spectra were recorded on a Jasco V-630 spectrophotometer. Steady-state emission experiments were carried out on a Shimadzu RF-5301 spectrofluorimeter at room temperature. The infrared spectra of solid samples dispersed in KBr were recorded on a Shimadzu FTIR-8400 spectrophotometer. The ^{1}H NMR spectrum was recorded on a Varian-Mercury 300 MHz spectrometer with DMSO-d_6 as the solvent at room temperature, and all chemical shifts are given relative to TMS. The electrospray ionization mass spectra were recorded on a Micromass Quattro II triple quadrupole mass spectrometer using acetonitrile/methanol as the solvent. Microanalyses (C, H, and N) were carried out with a ThermoQuest microanalysis instrument capable of carrying out CHNS (carbon, hydrogen, nitrogen, and sulfur) analysis. The cyclic voltammetric measurements were performed on a CH-electrochemical analyzer model 1100A with a conventional three-electrode cell assembly with a saturated Ag/AgCl reference electrode, a glassy carbon electrode as the working electrode ,and a platinum wire as an auxiliary electrode for all measurements in the presence of tetrabutylammonium perchlorate as the supporting electrolyte in dimethyl sulfoxide. The solutions were degassed for 1 h and blanketed with N_2 prior to measurements. Emission quantum yields (Φ) were calculated by integrating the area under the fluorescence curves and by using the following formula[44]

$$\Phi_{sample} = \left(\frac{OD_{standard}}{OD_{sample}}\right)\left(\frac{A_{sample}}{A_{standard}}\right)\Phi_{standard} \quad (1)$$

where OD is the optical density of the compound at the excitation wavelength (370 nm) and A is the area under the emission spectral curve. The standard used for the fluorescence quantum yield measurements was anthracene.[45] Radiative (k_r) and nonradiative (k_{nr}) decay rate constants were determined using the values of τ and Φ_r (radiative quantum yield) estimated at room temperature (Table 1).[44]

X-ray Crystallography. Single crystals of the ATSC (**1**) were grown by slow evaporation of the solution of compound in DMSO/ACN (4:1). Data was collected on SMART APEX-II CCD using Mo Kα radiation (λ = 0.7107 Å) to a maximum θ range of 25.00°. Yellow-orange rod-like crystals of approximatly 0.4 × 0.35 × 0.20 mm^3 in size were used for data collection. Crystal-to-detector distance = 5.00 cm; 512 × 512 pixels/frame; oscillation/frame = −0.5°; maximum detector swing angle = −30.0°; beam center = (260.2, 252.5); in-plane spot width = 1.24; multirun data acquisition. Total scans = 5; total frames = 1735; exposure/frame = 10.0 s/frame; θ range = 2.06−25.00°; completeness to θ of 25.00° = 99.8%. Largest diff. peak and hole = 0.592 and −0.389 e. $Å^{-3}$, respectively. All of the data were corrected for Lorentzian, polarization, and absorption effects. SHELX-97 (ShelxTL)[46] was used for structure solution and full matrix least-squares refinement on F^2. Hydrogen atoms were included in the refinement as per the

dx.doi.org/10.1021/bc400385d | Bioconjugate Chem. 2014, 25, 102−114

riding model. Data collection and refinement parameters are listed in Table 2.

Table 2. Crystal Data and Structure Refinement for 1

empirical formula	$C_{16}H_{13}N_3S$	
formula weight	279.36	
temperature	296(2) K	
wavelength	0.71073 Å	
crystal system	monoclinic	
space group	$P2_1$	
unit cell dimensions	a = 6.0514(1) Å	α = 90°
	b = 30.4883(5) Å	β = 94.4780(7)°
	c = 9.9339(2) Å	γ = 90°
volume	1827.18(6) Å^3	
Z	4	
density (calculated)	1.300 g/cm^3	
absorption coefficient	0.301 mm^{-1}	
F(000)	752	
crystal size	0.40 × 0.35 × 0.20 mm^3	
theta range for data collection	2.06−25.00°	
index ranges	$-7 \le h \le 7$, $-29 \le k \le 36$, $-11 \le l \le 11$	
reflections collected	12 217	
independent reflections	5597 [R_{int} = 0.0296]	
completeness to theta	25.00°, 99.8%	
absorption correction	semiempirical from equivalents	
max and min transmission	0.9423 and 0.8891	
refinement method	full-matrix least-squares on F^2	
data/restraints/parameters	5597/1/437	
goodness-of-fit on F^2	1.040	
final R indices [$I > 2\sigma(I)$]	R1 = 0.0477, wR2 = 0.1235	
R indices (all data)	R1 = 0.0540, wR2 = 0.1289	
absolute structure parameter	0.57(10)	
largest diff. peak and hole	0.592 and −0.389 eÅ^{-3}	

Crystallographic data in CIF format for the structures was deposited at the Cambridge Crystallographic Data Centre under CCDC ID 948039 for **1**. This data can be obtained free of charge via http://www.ccdc.cam.ac.uk/conts/retrieving.html or from the Cambridge Crystallographic Data Centre, 12 Union Road, Cambridge CB2 1EZ, UK; fax: (+44) 1223-336-033; or e-mail: deposit@ccdc.cam.ac.uk.

DNA Binding. The DNA-binding experiments were carried out in phosphate buffer (pH 7.2) using a 10% DMSO solution of **1** and **2** at room temperature. The ratio of the UV absorbance at 260 and 280 nm of a solution of calf thymus (CT) DNA in the buffer was found to be 1.8:1, indicating that the DNA was sufficiently free from protein. The concentration of CT DNA was estimated from its absorption intensity at 260 nm (ε = 6600 M^{-1} cm^{-1}). To obtain intrinsic binding constant, data were fitted to eq 2

$$[\mathrm{DNA}]/[\varepsilon_a - \varepsilon_f] = [\mathrm{DNA}]/[\varepsilon_b - \varepsilon_f] + 1/K_b[\varepsilon_b - \varepsilon_f] \quad (2)$$

where [DNA] is the concentration of DNA in base pairs, ε_a is the extinction coefficient observed for the absorption band at the given DNA concentration, ε_f is the extinction coefficient of the complex free in solution, and ε_b is the extinction coefficient of the complex when fully bound to DNA. A plot of $[\mathrm{DNA}]/[\varepsilon_a - \varepsilon_f]$ versus [DNA] gave a slope of $1/[\varepsilon_a - \varepsilon_f]$ and a y intercept equal to $(1/K_b)[\varepsilon_b - \varepsilon_f]$. The intrinsic binding constant K_b is the ratio of the slope to the intercept.

Fluorescence quenching experiments were carried out by the successive additions of 0 −50 μM of **1** and **2** to the DNA (10 μM) solutions containing 10 μM ethidium bromide (EtBr) in phosphate buffer. The changes in fluorescence intensities at 585 nm (545 nm excitation) of EtBr bound to DNA were recorded.

Viscosity Measurements. The viscosity experiments were carried out using a semimicro viscometer maintained at 30 °C in a thermostatic water bath. The flow time of the solutions in a phosphate buffer was recorded in triplicate for each sample, and an average flow time was calculated. Data were presented as $(\eta/\eta_0)^{1/3}$ versus the binding ratio, where η is the viscosity of DNA in the presence of compounds and η_0 is the viscosity of DNA alone.

DNA-Cleavage Studies. The cleavage of pBR322 DNA was performed in Tris−Boric acid−EDTA (TBE) buffer (pH 8.2) by treating DNA with **1** and **2** as per a reported procedure.[47] A total volume of 10 μL of sample solution was incubated in a sealed Eppendorf tube at 37 °C for 30 min followed by irradiation (365 nm) for 30 min. Then, 2 μL of loading buffer (0.025% bromophenol blue, 0.025% xylene cyanol, 2 mM EDTA, and glycerol) was added. The sample was then loaded onto a 1% agarose gel and electrophoresed at a constant voltage of 60 V for 3 h in TBE buffer (pH 8.2). The gel was stained with 0.5 μg/mL of ethidium bromide, visualized under UV light, and photographed for analysis. The extent of cleavage of the SC DNA was determined by measuring the intensities of the bands using the Alpha Innotech gel documentation system (AlphaImager 2200). For investigation of the mechanism, experiments were carried out in the presence of different radical-scavenging agents. These reactions were carried out by adding scavenging agents such as DMSO, mannitol, DABCO, L-histidine, sodium azide, and SOD to SC DNA prior to the addition of the complex and ligand. The concentrations of scavenging agents given in parentheses in the caption of Figure 7 correspond to the stock concentration.

BSA Interaction Studies. Quenching of the tryptophan residues of BSA was performed using **1** and **2** as quenchers. To solutions of BSA in phosphate buffer at pH 7.2 was added increments of the quenchers, and the emission signals at 345 nm (excitation wavelength at 295 nm) were recorded after each addition of the quencher.[48,49]

Anticancer Activity. *Maintenance of Cancer Cell Lines.* The HeLa (human cervical cancer) cell line was obtained from National Centre for Cell Sciences Repository, University of Pune, Pune, India. The cells were maintained in Dulbecco's minimum essential medium (DMEM) with 10% FBS and 0.1% antibiotic solution (complete medium, CM) at 37 °C with 5% CO_2 in a stericycle CO_2 incubator with HEPA class 100 filters (Thermo Electron Corporation).

Preparation of Samples for Cell Line Testing. The compounds were dissolved in 10% DMSO to obtain a solution of 1 mM each. The samples were then diluted to 100 μM in PBS solution and filter-sterilized using a 0.22 μm syringe filter. This 100 μM solution in PBS was further used in cell cytotoxicity studies. The cells, trypsinized using TPVG solution (1×10^5 cells/mL), were seeded in a 96-well plate. A range of concentrations of the compounds diluted in CM were added to the cells and incubated at 37 °C in a CO_2 incubator for 24 h. After the incubation, the cells were visualized using an inverted Olympus microscope. All experiments were carried out in laminar flow hoods (Laminar Flow Ultraclean Air Unit, Microfilt, India).

Protocol for MTT Assay. A solution of 5 mg/mL MTT was dissolved in PBS and filter-sterilized using a syringe filter. After incubation for the stipulated time, 20 μL of MTT solution was added to 200 μL of cell content solution. The plate was incubated for 2 h in the CO_2 incubator. After incubation, the media was removed, 200 μL of DMSO was added to each well to dissolve the crystals, and the plate was placed into the incubator at 37 °C for 5 min. A reading was taken on a plate reader (Thermo Electron Corporation), measuring the absorbance at 540 and 620 nm.

Cell Staining for Flow Cytometry. For preparation of cells for FACS, the APO-BrDU TUNEL assay kit from Invitrogen was used. HeLa cells were plated on 6-well plates. The wells were designated as unstained control, control (without any treatment), and only PBS added. Compounds **1** and **2** were added at 25 μM. The plates were incubated for 24 h, and the cells were fixed briefly according to the kit's protocol. For cell fixation, cells were suspended in 1% paraformaldehyde in PBS (pH 7.4) at a concentration of $1-2 \times 10^6$ cells/mL, which was kept on ice for 30 min. Then, the fixed cells were centrifuged at 300*g* for 5 min, the supernatant was decanted, and the cells were washed in 5 mL of PBS and resuspended in residual PBS. The cells were mixed with 70% ice-cold ethanol and stored in freezer at −20 °C for 24 h. For cell staining, cells were resuspended in 1 mL of wash buffer and then centrifuged, and the supernatant was removed. Wash buffer treatment was repeated. Cells were resuspended in 50 μL of DNA-labeling solution (containing TdT reaction buffer, TdT enzyme, Br-dUTP,and distilled water) for 60 min at 37 °C by shaking every 15 min to resuspend. Then, 1 mL of rinse buffer was added to each tube, and the samples were centrifuged at 300*g* for 5 min. The supernatant was removed, and the rinse-buffer treatment was repeated. Cells were resuspended in 1 mL of antibody solution (containing Fluorescein PRB-1 and rinse buffer) and incubated in the dark for 30 min at room temperature. Then, 0.3 mL of propidium iodide/RNase A solution was added to each tube followed by incubation in the dark for 30 min at room temperature. Cells were analyzed for DNA damage and cell cycle checkpoints for apoptosis using flow cytometry analysis.

Flow Cytometry. The cells were counterstained with PI according to the kit instructions and analyzed on a Calibur FACScan flow cytometer (Becton Dickinson; San Jose, CA). PI fluorescence was acquired using linear amplification into FL3 (630LP) and log amplification into FL2 (585/20BP). Green fluorescence was acquired using log amplification into FL1 (530/30BP). A minimum of 10 000 events were collected for each sample. TUNEL-positive cells were quantified as the percentage of doublet-gated PI-positive cells. Sub-G1 apoptotic events with degraded DNA were not distinguishable from debris and were excluded from analysis. The fluorescence level for discrimination between apoptotic and nonapoptotic cells was set using the control without TdT. Cells above this fluorescence value in the TdT-positive sample were considered apoptotic. Analysis was performed using CellQuest Pro software (Becton Dickinson).

Protocol for Cell Fixation. Cells were trypsinized and suspended in 0.5 mL PBS. The cell suspension was added to 5 mL of 1% paraformaldehyde (w/v) in PBS and placed on ice for 15 min. The cells were centrifuged at 300*g* for 5 min, and the supernatant was discarded. The cells were washed with 5 mL of PBS, pelleted again by centrifugation, resuspended in 0.5 mL PBS, and then added to ice-cold 70% ethanol (v/v). The cells were stored at −20 °C until further use. The cells were stained per the protocol in the Invitrogen APO-BrdU TUNEL assay kit. The FACS analysis data was acquired using BD FACS Calibur. The data was analyzed using CellQuest Pro software.

RESULTS AND DISCUSSIONS

Synthesis and Characterization. Anthracene thiosemicarbazone, ATSC (**1**), was prepared by condensation of anthraldehyde and thiosemicarbazide in the presence of glacial acetic acid. Its structure was confirmed by elemental analysis, ESI-MS, ^{1}H NMR, and single-crystal X-ray structure. The corresponding copper(II) complex (**2**) was synthesized as described in the Experimental Procedures (Scheme 1). The

Scheme 1. Synthetic Scheme of ATSC and Its Corresponding Copper Complex

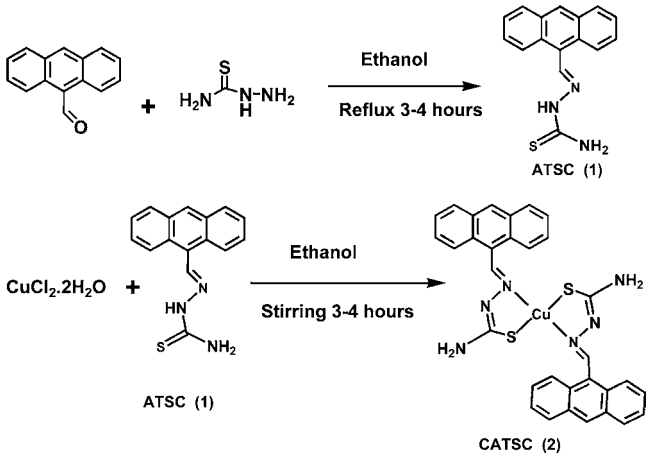

positive-mode ESI-MS analysis of **1** showed a peak at m/z 280 for $[M + H]^+$, and **2** gave a peak at m/z 736.2, corresponding to $[M + H + 2ACN + MeOH]^+$, revealing that the identity of the complex is retained in solution. The photophysical properties of **1** and **2** are summarized in Table 1. The UV−vis spectra (Figure 1A) of **1** and **2** were recorded in dimethyl sulfoxide (DMSO). Intense absorption bands in the range of 350−450 nm in the UV−vis spectra of **1** and **2** are assigned to the intraligand $\pi \rightarrow \pi^*$ transitions in anthracene. The low-energy band centered at 690 nm in **2** is attributed to the d → d transitions typical of copper(II) complexes.[49,50] As shown in Figure 1B, the emission spectra of **1** and **2** recorded in DMSO show a structureless broad peak at 500 nm and a shoulder at 484 nm in **1** when excited at 370 nm. This can be attributed to the formation an intramolecular exciplex because of the partial charge transfer from the thiosemicarbazide group to anthracene. The emission quantum yields of **1** and **2** along with the radiative and nonradiative rate constants are tabulated in Table 1. The decays were fitted to a biexponantial profile. For **1**, the short-lived component at 2.05 ns (45.49%) is assigned to the emission of monomeric compound, and the long-lived component at 7.44 ns (54.51%), the excimer emission. For **2**, the short-lived component decays in 2.28 ns (42.51%), whereas long-lived component decays slowly with a lifetime of 9.25 ns (57.49%). Sharp bands at 1601 and 846 cm^{-1} in the IR spectrum of **1** are assigned to ν(C═N) and ν(C═S), respectively. The shift in these bands to lower wavenumbers on complexation suggests that thiosemicarbazone binds to copper through sulfur and the azomethinic nitrogen,

dx.doi.org/10.1021/bc400385d | *Bioconjugate Chem.* 2014, 25, 102−114

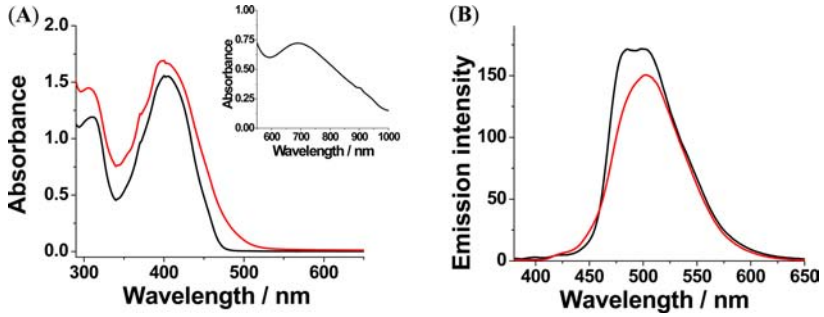

Figure 1. Absorption (A) and emission spectra (B) of **1** (black) and **2** (red) in DMSO solvent.

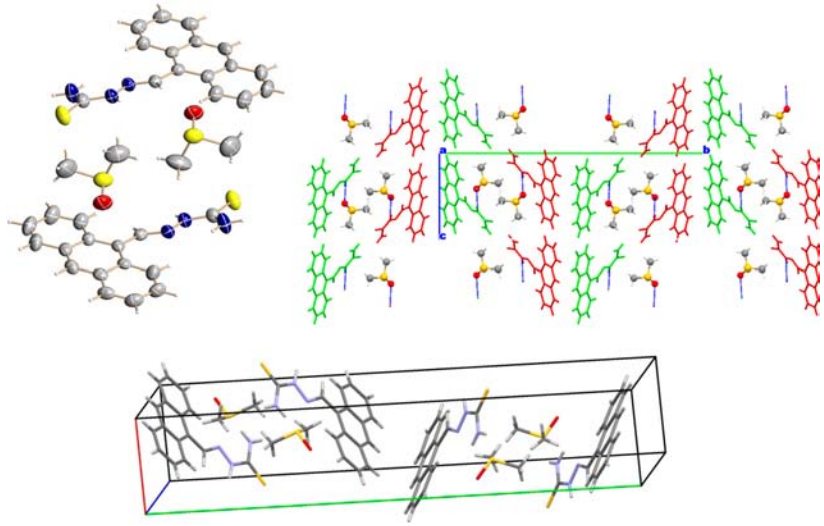

Figure 2. ORTEP and packing diagram of ATSC (**1**).

Table 3. Electrochemical Data for 1 and 2

compound	oxidation peaks (V)	assignment	reduction peaks (V)	assignment	ref
9,10-diphenylanthracene (DPA)[a]	1.18 (rev)[a] 1.50 (irr)[a]	$DPA^{+\bullet}$ DPA^{2+}	−1.8	$DPA^{-\bullet}$	58
DPA[e]	1.25[a] 1.22[b] (rev) 1.60[b] (irr)	$DPA^{+\bullet}$ $DPA^{+\bullet}$ DPA^{2+}	−1.95 −1.8 to −2.0	$DPA^{-\bullet}$ $DPA^{-\bullet}$	59
anthracene			−1.41[b] −1.88[b]		60
9,10-acetoxyanthracene			−1.19[b] −1.65[b]		60
$[Rh(acac)_2(anCH_2acac)]$	1.67[c] (rev)	oxidation of anthryl group	−2.14 (rev)[c] −2.85 (irr)[c]	$Anth^{-\bullet}$ $Anth^{2-}$	54
$[Rh(acac)_2(anCOacac)]$	1.62[c]	oxidation of anthryl group	−2.01 (irr)[c] −2.90 (rev)[c]	$Anth^{-\bullet}$ $Anth^{2-}$	54
$[Ir(acac)_2(anCH_2acac)]$	1.35[c]	oxidation of anthryl group	−1.97 (rev)[c]	reduction of anthrylene moiety	54
$[Ir(acac)_2(anCOacac)]$	1.45[c]	oxidation of anthryl group	−1.66 (irr)[c]	dimerization of anthryl moiety	54
ATSC, **1**	1.03 (QR)[f]	oxidation of anthryl group	−1.45 (irr) −1.70 (rev) −2.23 (QR)	anthryl dimerization $Anth^{-\bullet}$ $Anth^{2-}$	Present work
CuATSC, **2**	0.31 (QR)[f]	Cu(II)−Cu(I)	−1.85 (rev) −2.44 (irr)	$Anth^{-\bullet}$ $Anth^{2-}$	Present work

[a]Acetonitrile. [b]DMF, referenced vs a dropping-mercury electrode. [c]THF, referenced vs Ag/AgCl. [d]DMSO. [e]Referenced vs SCE. [f]DMSO, referenced vs Ag/AgCl; rev = reversible; irr = irreversible; QR = quasi reversible; $Anth^{-\bullet}$ = anthryl radical anion; $Anth^{2-}$ = anthryl dianion; $DPA^{+\bullet}$ = diphenylanthracene radical cation; DPA^{2+} = diphenylanthracene dication; $DPA^{-\bullet}$ = diphenylanthracene radical anion; and DPA^{2-} = diphenylanthracene dianion.

which deprotonates on binding to copper, resulting in bond delocalization.[51]

Crystal Structure of ATSC (1). Crystals suitable for X-ray structure determination of **1** were obtained by slow evaporation in DMSO/acetonitrile (4:1) at room temperature. An ORTEP representation of **1** is shown in Figure 2. A summary of the crystallographic data is compiled in Table 2, and bond lengths and bond angles are given in Table S1. The compound

dx.doi.org/10.1021/bc400385d | *Bioconjugate Chem.* 2014, 25, 102−114

crystallizes in the monoclinic space group $P2_1$, with two molecules in the asymmetric unit. The molecules form a dimer via intermolecular N−H···S hydrogen-bonding interactions. DMSO molecules are sandwiched between two symmetry-related molecules when viewed down the *a* axis. The planar anthracene rings are at distances of 3.165 and 3.276 Å for the two symmetrically related molecules in the asymmetric unit, showing $\pi-\pi$ interactions (Supporting Information, Figure S1). The ATSC molecules are held together by DMSO solvent molecules with C−H···O and N−H···O interactions. The distance of N3···S1 is 3.409 Å and H3B···S is 2.58 Å, and the angle of N3−H3B···S1 is 163°. These bond lengths and angles are in accordance with the ethyl-substituted anthracene thiosemicarbazone reported by Yan et al.[52]

Electrochemistry. Electrochemical studies of **1** and **2** were carried out in dry dimethyl sulphoxide using a glassy carbon working electrode and a platinum wire auxiliary electrode with tetrabutylammonium perchlorate as the supporting electrolyte. All of the potentials were referenced to the standard Ag/AgCl reference electrode. Voltammetric data for **1** and **2** are presented in Table 3, and cyclic voltammograms are displayed in Figures S2 and S3. The first irreversible reduction in **1** located at −1.45 V indicates dimerization of a reduced anthryl moiety.[53] Two additional reduction peaks at −1.70 (reversible, with peak-to-peak separation of 87.5 mV) and −2.23 V (quasi reversible, with peak to peak separation of 213 mV) are attributed to the radical anion and dianion of the anthryl group, respectively.[54] A one-electron oxidation peak is observed at +1.03 V, which can be assigned to the oxidation of the anthryl group.[55,56] On copper complexation, dimerization of anthracene is inhibited, which is reflected in the absence of the corresponding peak in the voltammogram of **2**. Furthermore, formation of the anthracene anion radical and dianion was found to be delayed. An additional peak centered at +0.31 V is assigned to the $Cu^{II}-Cu^{I}$ redox couple. The positive redox potential suggests faster release of copper from **2** compared to Cu(ATSM) and Cu(GTSM).[57] The change in the position and shape of the oxidation and reduction peaks in **2** suggests significant intramolecular interaction between copper(II) and the anthryl moiety, which promotes the incoming electrons to the metal center through its reduction.

DNA-Binding Studies. The investigation of the binding of metal complexes to DNA is of prime importance in the development of anticancer drugs.[61] The DNA-binding ability of **1** and **2** to CT DNA was studied using UV−vis spectroscopy. Changes observed in the intraligand absorption band (250−450 nm) of **1** and **2** exhibit significant hypochromicity (18 and 12%, Table 4) as a function of increased DNA concentration (Figure S4). The binding strengths of the compounds with DNA were determined using eq 2 and were found to be $2.6 \pm 0.2 \times 10^4$ and $3.8 \pm 0.1 \times 10^5$ for **1** and **2**, respectively, suggesting considerably moderate binding with DNA because the extent of hypochromism is usually associated with the strength of DNA interaction.[62−64]

Ethidium Bromide-Displacement Assay. Competitive binding studies using ethidium bromide (EtBr) bound to DNA were carried out for **1** and **2**. In buffer medium, ethidium bromide fluorescence is quenched by solvent molecules and increases about 20-fold after binding to DNA.[65,66] The emission intensity of EtBr bound DNA will be quenched by the addition of a quencher, which is a result of the displacement of ethidium bromide bound to DNA. Figure 3 shows the emission spectra when **1** and **2** were added to DNA pretreated with EtBr ([DNA]/[EtBr] = 1:1). It was observed that there is a decrease in the fluorescence intensity at λ_{em} 585 nm with increased concentration of **1** and **2**. However, the effect of **2** is stronger. The lower DNA-binding affinity of **1** suggests partial intercalation or surface binding because of a decrease in the planarity of the free ligand, leading to the formation of bends or kinks in DNA.[67] The apparent binding constant, K_{app}, was calculated using the following equation

$$K_{EtBr}[EtBr] = K_{app}[M_{50\%}] \quad (3)$$

where $[M_{50\%}]$ is the concentration of the ligand and metal at 50% reduction of fluorescence and K_{EtBr} is the binding constant for ethidium bromide. The concentration of ethidium bromide is 10 μM. The K_{app} value for **2** was found to be 2.1×10^6, which is higher, indicating strong binding with DNA. The K_{app} value for **1** could not be calculated because of the lack of 50% reduction of EB emission in the concentration range used in the present study.

Table 4. Electronic Absorption Data upon Addition of CT-DNA

compound[a]	hypochromism, H (%)[b]	K_b (M^{-1})[b]
1	18	$2.6 \pm 0.2 \times 10^4$
2	12	$3.8 \pm 0.1 \times 10^5$
9-anthrylmethylammonium chloride[27,a]		1.4×10^4
9-anthrylpropylammonium chloride[27,a]		1.5×10^4
anthracene derivative of 1,8-octyldiamine (AODA)[27,a]		5.3×10^5

[a][**1**] and [**2**] = 20 μM. [b]H (%) = $100(A_{free} - A_{bound})/A_{free}$ in phosphate buffer (pH 7.2), where *A* is the absorbance.

Viscosity Studies. To understand the mode of binding with DNA, the viscosity of CT DNA solutions containing varying amounts of **1** and **2** were measured. The length of the DNA helix increases upon intercalation as base pairs are separated to accommodate the binding ligand, which results in the increased viscosity of the DNA. In this study, DNA solutions (100 μM) containing 0−50 μM of **1** and **2** were placed in the viscometer, and flow times were measured after thermal equilibrium (Figure 4). With increased concentration, **2** displayed a linear increase in the viscosity of the CT DNA. However, at lower binding ratios ($r < 0.2$) **1** showed decrease in viscosity, which increased gradually upon further increasing molar ratio (r).[68] Thus, together with the results from the EtBr displacement experiments, we conclude that **1** and **2** are partial intercalators.

DNA-Cleavage Studies. The cleavage of plasmid pBR322 DNA by **1** and **2** was carried out using 1% agarose gel electrophoresis in TBE buffer (pH 8.2). When incubated in the dark, compounds did not show any DNA cleavage (Figure S4). On irradiation with monochromatic UV light of 365 nm, **1** and **2** cleave DNA efficiently, with the complete conversion of supercoiled form I into nicked circular form II (Figures 5 and 6) at 10 and 20 μM concentrations, respectively, after 30 min of irradiation followed by a 30 min incubation at 37 °C. A small percentage of linear DNA was also observed.

To investigate the mechanism involved in the DNA cleavage upon photoirradiation, **1** and **2** were incubated in the presence of different reactive-oxygen scavengers (Figure 7). There was no appreciable effect on DNA cleavage by **1** in the presence of DMSO, mannitol, and SOD, whereas addition of DABCO, L-

dx.doi.org/10.1021/bc400385d | Bioconjugate Chem. 2014, 25, 102−114

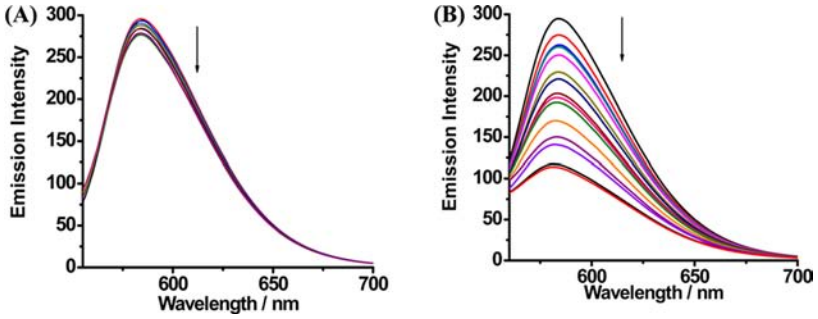

Figure 3. Effect of addition of **1** (A) and **2** (B) on the emission intensity of the CT DNA-bound ethidium bromide (10 μM) at different concentrations in 10% DMSO in phosphate buffer (pH 7.2).

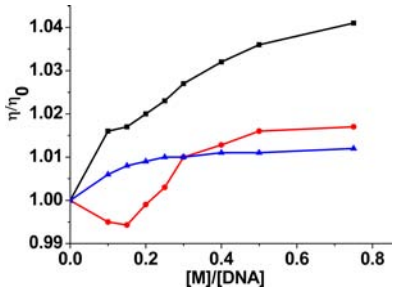

Figure 4. Effect of increasing the amount of EtBr (black line), **1** (red line), and **2** (blue line) on the relative viscosities of calf thymus DNA at 28 °C. [DNA] = 100 μM.

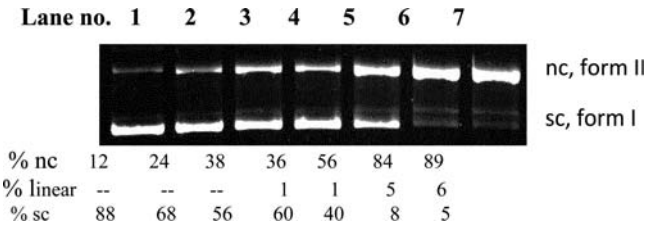

Figure 5. Photograph of a 1% agarose gel showing cleavage of plasmid pBR 322 DNA by **1** after incubation for 30 min at 37 °C followed by irradiation at 365 nm for 30 min. [DNA] = 300 ng. Lane 1 = DNA control; 2 = DNA + **1** (2 μM); 3 = DNA + **1** (4 μM); 4 = DNA + **1** (6 μM); 5 = DNA + **1** (8 μM); 6 = DNA + **1** (10 μM); and 7 = DNA + **1** (20 μM).

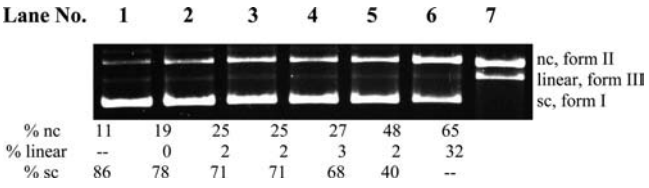

Figure 6. Photograph of a 1% agarose gel showing cleavage of plasmid pBR 322 DNA by **2** after incubation for 30 min at 37 °C followed by irradiation at 365 nm for 30 min. [DNA] = 300 ng. Lane 1 = DNA control; 2 = DNA + **2** (2 μM); 3 = DNA + **2** (4 μM); 4 = DNA + **2** (6 μM); 5 = DNA + **2** (8 μM); 6 = DNA + **2** (10 μM); and 7 = DNA + **2** (20 μM).

histidine, and sodium azide reduced the DNA cleavage by ~20, 37, and 61%, respectively (Figure 7A, lanes 5–7). These results suggest that singlet oxygen is responsible for the DNA damage caused by **1**. When **2** is incubated with different reactive-oxygen scavengers, inhibition of DNA cleavage was observed in the presence of L-histidine (82%, lane 6) and to some extent in the presence of sodium azide, suggesting the involvement of singlet oxygen in DNA cleavage by the copper(II) complex.

BSA Interaction Studies. Serum albumin constitutes about 55% of total plasma proteins and plays a pivotal role in the transport of drug and their metabolism.[44,69] BSA is the most studied serum albumin because of its homology with human serum albumin (HSA). It exhibits intrinsic fluorescence because of the presence of aromatic amino acids phenylalanine, tyrosine, and tryptophan. If the tyrosine is ionized, then its fluorescence is completely quenched, whereas phenylalanine has a very low quantum yield. This means that intrinsic fluorescence of BSA is due to tryptophan alone. Figure 8 shows the effect of increasing the concentration of **1** and **2** on the fluorescence emission of BSA. A steady decrease in the characteristic emission band centered at 345 nm was observed with the increasing concentration of **1** and **2**. Quenching of emission can result from various molecular interactions like excited-state reactions, molecular rearrangements, energy transfer, ground-state complex formation, and collisional quenching. Quenching can occur by different mechanisms, usually classified as either static or dynamic quenching, and can be discriminated by its dependence on temperature and excited-state lifetime. Higher temperature results in faster diffusion and hence larger collisions between fluorophore and quencher, resulting in increased K_{sv}, which is termed dynamic quenching. However, in static quenching, higher temperatures will result in dissociation of the ground-state complex between the fluorophore and quencher, leading to decreased stability constants and lower values of quenching constants. The decrease in intensity is described by Stern–Volmer eq 4

$$(F_0/F) = 1 + K_{sv}[Q] = 1 + K_q\tau_0[Q] \quad (4)$$

where F_0 and F are the steady-state fluorescence intensities in the absence and presence of quencher, respectively, K_{sv} is the Stern–Volmer quenching constant, [Q] is the concentration of quencher, K_q is the quenching rate constant, and τ_0 is the average lifetime of the biomolecule without quencher (about 10^{-8} s) .

The calculated values of K_{sv} and k_q at various temperatures are given in Table 5 (calculated from Stern–Volmer plots, Figure S6). These results show a static quenching mechanism for **1** because the quenching constant decreases with the increase in temperature. However, quenching constant increases with an increase in temperature indicate the dynamic quenching mechanism for **2**. Furthermore, the quenching rate constant, K_q, for interaction of **1** and **2** with BSA was found to be greater than the K_q of scatter collisional quenching of other quencher–biomolecular interactions reported in the litera-

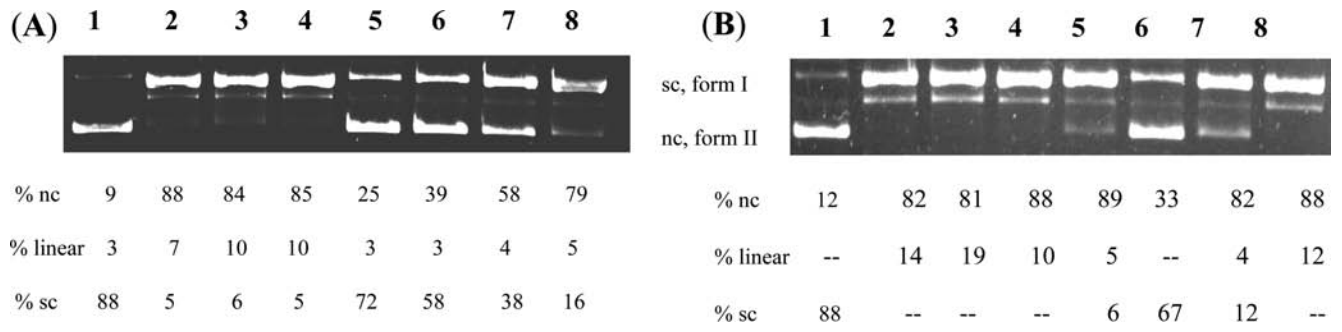

Figure 7. Photograph of a 1% agarose gel showing the effect of inhibitors on cleavage of pBR322 plasmid DNA by (A) **1** [DNA] = 300 ng, [**1**] = 10 μM. Lane 1 = DNA control; 2 = DNA + **1**; 3 = DNA + **1** + DMSO; 4 = DNA + **1** + mannitol (50 mM); 5 = DNA + **1** + DABCO (10 mM); 6 = DNA + **1** + L-histidine (20 mM); 7 = DNA + **1** + NaN_3 (20 mM); and 8 = DNA + **1** + SOD (15 units). (B) [**2**] = 20 μM. Lane 1 = DNA control; 2 = DNA + **2**; 3 = DNA + **2** + DMSO; 4 = DNA + **2** + mannitol (50 mM); 5 = DNA + **2** + DABCO (10 mM); 6 = DNA + **2** + L-histidine (20 mM); 7 = DNA + **2** + NaN_3 (20 mM); and 8 = DNA + **2** + SOD (15 units).

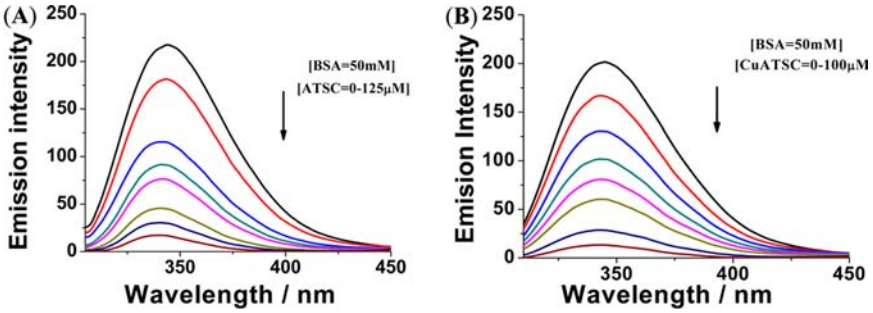

Figure 8. Effect of addition of (A) **1** and (B) **2** on the emission intensity of BSA (50 μM) at different concentrations in a 20% DMF phosphate buffer (pH 7.2).

Table 5. Stern–Volmer Quenching Constants, Quenching Rate Constants, and Relative Thermodynamic Parameters for 1 and 2 at Different Temperatures

compound	T (K)	$K_{SV} \times 10^4$ (M^{-1})	$K_q \times 10^{12}$ (M^{-1} s^{-1})	$K_b \times 10^4$ (M^{-1})	n	ΔG (kJ mol^{-1})	ΔH (kJ mol^{-1})	ΔS (J mol^{-1} K^{-1})
1	301	4.9	4.9	2.3	1.9	−25.1	−4.8	73.9
	309	4.7	4.7	2.9	1.9	−26.4		
	317	4.5	4.5	3.6	1.7	−27.6		
2	301	3.4	3.4	1.4	2.0	−23.8	2.9	97.4
	309	3.9	3.9	1.1	1.9	−23.9		
	317	4.0	4.0	1.2	2.0	−24.7		

ture,[70] implying that the quenching is not initiated by dynamic collisions but from the formation of a complex.[71]

The thermodynamic parameters calculated from a van't Hoff plot (Figure S7) are tabulated in Table 5. The negative sign for the free energy (ΔG) indicates that the binding process is spontaneous. The small negative enthalpy value for **1** and positive entropy change (+73.91 J mol^{-1} K^{-1}) demonstrate the major role of hydrophobic and electrostatic interactions in binding.[72] The positive enthalpy (ΔH) and entropy (ΔS) values for the interaction of **2** with BSA point toward an entropy-driven process, for which enthalpy is not favorable and hydrophobic forces play a major role in the reaction.[72,73] The binding constants for the interaction of BSA with **1** and **2** were on the order of 10^4, which is neither too weak nor too strong for the transport and release of protein-bound compounds through biological fluids at the cellular level to exhibit anticancer activity (Figure S8).[74] The number of binding sites are approximately equal to two, suggesting the binding of two molecules of **1** and **2** with one molecule of BSA.

Cytotoxicity Study and Cellular Uptake. *MTT Assay.* MTT assay was performed to determine the ability of **1** and **2** to inhibit cell growth and induce cell death in HeLa (human cervical carcinoma) cells. As can be seen from Figure 9, compared to ligand **1**, its copper(II) complex (**2**) showed considerable cytotoxicity, with IC_{50} values of 22 and 15 μM,

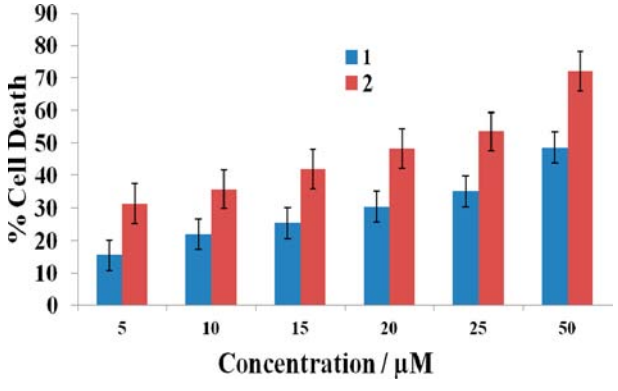

Figure 9. Effect of concentration on the death of HeLa cells by **1** and **2** as determined by MTT assay.

dx.doi.org/10.1021/bc400385d | *Bioconjugate Chem.* 2014, 25, 102–114

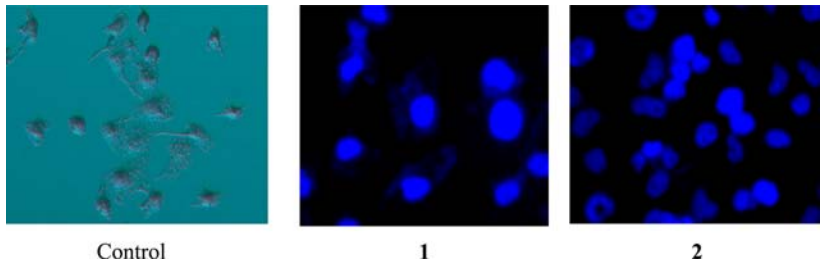

Figure 10. Cellular uptake of **1** and **2** by HeLa cells monitored after an 8 h incubation under a Zeiss Axioscope with filter set no. 2.

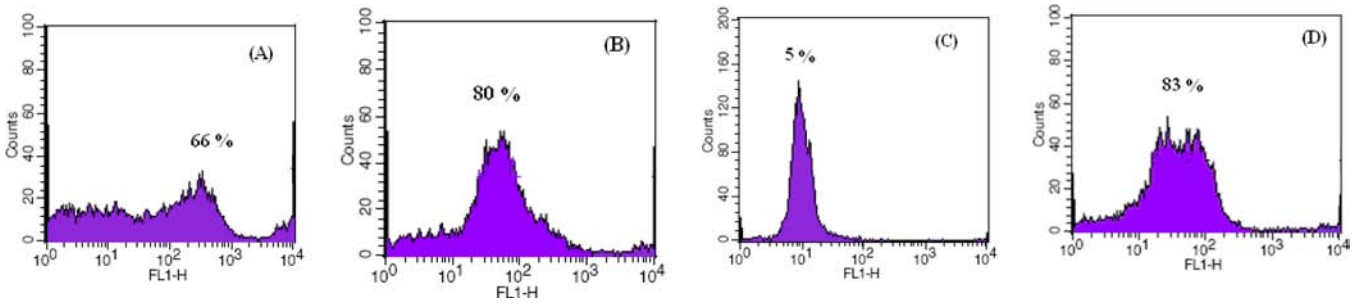

Figure 11. Apoptosis induced by (A) **1**, (B) **2**, (C) negative control, and (D) positive control.

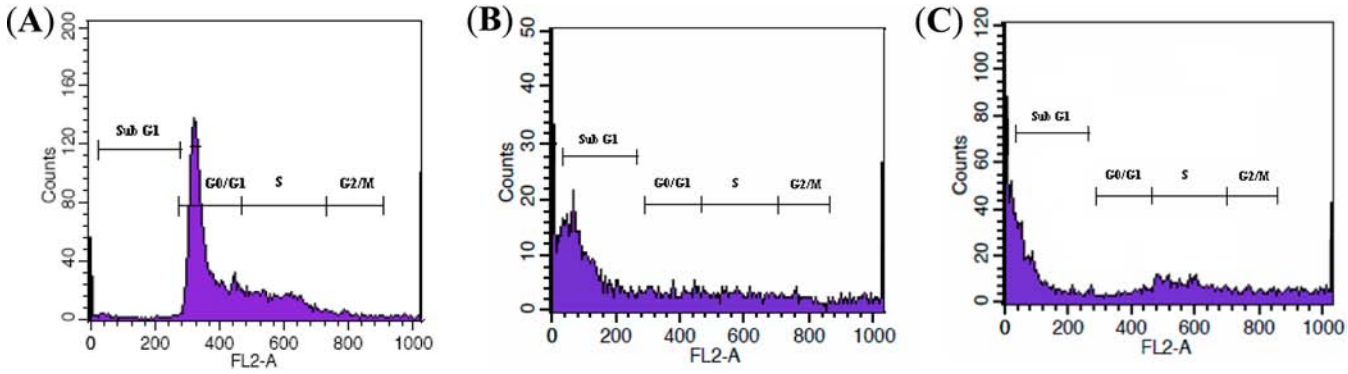

Figure 12. Effect of **1** and **2** on the cell cycle progression distribution of HeLa cells. The cell cycle phase was determined by the amount of DNA measured by flow cytometry of PI-stained cells. (A) Control, (B) **1**, and (C) **2**.

respectively. The amount of cell proliferation significantly decreased in a dose-dependent manner on supplementation with **1** and **2**, as observed within 24 h of incubation with the HeLa cells. Because thiosemicarnazones are known inhibitors of enzyme ribonucleotide diphosphate reductase (RDR),[75] the antiproliferative activity of **1** and **2** in the absence of irradiation can be attributed to the inhibition of RDR. RDR is responsible for maintaining a balanced supply of dNTPs required for DNA synthesis and repair and plays an important role in cell proliferation.[76,77] Inactivation of RDR in cells leads to decreased concentration of dNTPs, leading to inhibition of DNA synthesis and repair, cell cycle arrest, and apoptosis.[78,79] Tumor cells are more sensitive to the cytotoxic effects of RDR inhibition than normal cells. Hence, it is considered to be an excellent target for cancer chemotherapy.[78,80] Furthermore, it has been shown that the Fe(II) complex of 3-aminopyridine-2-carboxaldehyde thiosemicarbazone (3-AP, Triapine), a potent inhibitor of RDR currently in phase II clinical trials, activates molecular oxygen to produce reactive oxygen species and causes DNA degradation by acting not only as an RDR inhibitor but also as a DNA damaging agent.[81−83] The two functions can combine synergistically, causing cell cycle arrest and apoptosis. It is conjectured that a similar mechanism is responsible for the greater antiproliferative activity of **2** than **1** besides the variation in their cellular uptake.

Figure 10 shows the cellular uptake of **1** and **2** by HeLa cells monitored by fluorescence microscopy. Bright blue fluorescence was observed when cells were incubated with 25 μM **1** and **2** for 8 h at 37 °C, demonstrating their uptake by the cells. Interestingly, only the nucleus was found to be stained blue, suggesting that the nucleic acid is the main cellular target.

Mode of Cell Death. *Cell Staining for Detection of Changes in Morphology.* To determine the mode of cell death, cells were grown on coverslips, treated with the compounds for 6 h (Figure S9), and observed for changes in morphology. Control cells were stained with eosin. Staining after addition of compounds up to 24 h showed no changes in cell shape or size using a phase-contrast microscope. This indicated that the cell mode was not necrotic, as the cell structure integrity was intact. Hence, it was taken as the indication that the mode of cell death was most likely apoptosis, and further analysis by fluorescence-activated cell sorting (FACS) was carried out to confirm the mode of cell death.

dx.doi.org/10.1021/bc400385d | *Bioconjugate Chem.* 2014, 25, 102−114

For this, the TUNEL assay (terminal deoxynucleotide transferase dUTP nick end labeling assay) was used. During apoptosis, the DNA gets fragmented into small parts. In this assay, the enzyme terminal deoxynucleotidyl tranferase (TdT) transfers bromodeoxyuridine triphosphate (Br-UTP) to the ends of many fragments formed. A fluorescein-labled antiBrDU antibody is then used to count the fragments. Thus, greater dye intensity means a larger number of fragments, indicating a larger apoptotic cell population. Propidium iodide (PI) was also added to the sample because PI stains DNA and is an indicator of apoptosis. Thus, we checked for the dual-positive population (i.e., cells showing both fluorescien PRB-1 and PI staining), which indicates apoptotic cells.

From the histogram statistics for the PI intensity for **1** and **2** (Figure 11), the apoptotic population was calculated from the dual-positive cells (FL-1H and FL-2A). The percent of apoptosis for **1** was found to be 66 and 80% for **2**. This data is similar to the cytotoxicity data obtained from the MTT assay within 24 h of drug uptake. The values obtained were also confirmed with the dual-positive and -negative cells provided in the Invitrogen ApoBrdu kit, which are represented in the graph. Thus, it can be inferred that the number of apoptotic cells in cells treated with **2** are much greater than the apoptotic cells treated with **1**.

Cell Cycle Analysis. Cells treated with compounds **1** and **2** for 24 h were analyzed for cell cycle analysis to investigate the molecular mechanism behind cell growth inhibition using flow cytometry, which permits a quantitative estimation of the DNA content of cells. A representative of three independent experiments is shown in Figure 12. Interestingly, both compounds are able to arrest the cells at the S and G2/M phases and show an increased cell population in the sub-G1 phase, revealing an increase in apoptotic cell death.[49,84,85] Some of the compounds that are currently used in the clinic are known to exploit G1 arrest (e.g., clotrimazole), which induces late G1 cell cycle arrest in vitro.[86] Paclitaxel was also found to cause G1 arrest at concentrations of 3−6 nM in A549 lung cancer cells.[87]

CONCLUSIONS

Anthracene thiosemicarbazone (**1**) and copper(II) complex (**2**) were synthesized and characterized by various analytical techniques. DNA and protein binding and DNA cleavage of **1** and **2** were carried out by different techniques. Both **1** and **2** efficiently cleave plasmid pBR322 DNA upon photoirridation at 365 nm without addition of any external additives. Cellular uptake of **1** and **2** could be monitored by fluorescence microscopy because of the inherent fluorescence of anthracene. The effect of **1** and **2** is associated with cell cycle arrest in the sub-G1 phase. **2** is able to induce ∼80% apoptosis at a concentration of 25 μM within 24 h of incubation. Thus, it shows effective antiproliferative effects and has the potential to be developed as a chemotherapeutic agent for the treatment of cervical cancer.

ASSOCIATED CONTENT

Supporting Information

Selected bond angles and lengths for **1**; $\pi-\pi$-stacking interactions of the aromatic rings of the anthracene of **1**; cyclic voltammograms of **1** and **2**; changes in the electronic absorption spectra of **1** and **2** in the presence and absence of CT-DNA; DNA cleavage by **1** and **2** in the dark; Stern−Volmer plots for the interaction of BSA with **1** and **2** at various temperatures; van't Hoff plots and Lineweaver−Burk plots; cell staining with eosin for detection of changes in morphology; and procedures for calculating thermodynamic and binding parameters. This material is available free of charge via the Internet at http://pubs.acs.org.

AUTHOR INFORMATION

Corresponding Author

*E-mail: aak@chem.unipune.ac.in; Fax: (+91) 020 25691728.

Notes

The authors declare no competing financial interest.

ACKNOWLEDGMENTS

This work was sponsored by the Board of Research in Nuclear Sciences (BRNS), Department of Atomic Energy (DAE). A.N.K. acknowledges financial assistance in the form of a Junior Research Fellowship (JRF) from BRNS. A.A.Ku. acknowledges a BCUD seed grant (no. F/2012-13/637) for partial funding. We also thank the Central Drug and Research Institute (CDRI), Lucknow, India, for ESI-MS and elemental analyses. A.A.Kh. acknowledges the Institute of Bioinformatics and Biotechnology, University of Pune for providing the animal tissue culture facility.

REFERENCES

(1) Guo, Z., and Sadler, P. J. (1999) Metals in medicine. *Angew. Chem., Int. Ed. 38*, 1512−1531.
(2) Dyson, P. J., and Sava, G. (2006) Metal-based antitumour drugs in the post genomic era. *Dalton Trans.*, 1929−1933.
(3) Orvig, C., and Abrams, M. J. (1999) Medicinal inorganic chemistry: Introduction. *Chem. Rev. 99*, 2201−2204.
(4) Ho, Y.-P., Au-Yeung, S. C. F., and To, K. K.W. (2003) Platinum-based anticancer agents: Innovative design strategies and biological perspectives. *Med. Res. Rev. 23*, 633−655.
(5) Sherman, E. S., and Lippard, S. J. (1987) Structural aspects of platinum anticancer drug interactions with DNA. *Chem. Rev. 87*, 1153−1181.
(6) Williams, D. R. (1972) Metals, ligands, and cancer. *Chem. Rev. 72*, 203−213.
(7) Erkkila, K. E., Odom, D. T., and Barton, J. K. (1999) Recognition and reaction of metallointercalators with DNA. *Chem. Rev. 99*, 2777−2795.
(8) Romero-Canelón, I., and Sadler, P. J. (2013) Next-generation metal anticancer complexes: Multitargeting via redox modulation. *Inorg. Chem. 52*, 12276−12291.
(9) Bruijnincx, P. C. A., and Sadler, P. J. (2008) New trends for metal complexes with anticancer activity. *Curr. Opin. Chem. Biol. 12*, 197−206.
(10) Hannon, M. J. (2007) Metal-based anticancer drugs: From a past anchored in platinum chemistry to a post-genomic future of diverse chemistry and biology. *Pure Appl. Chem. 79*, 2243−2261.
(11) Zhang, C. X., and Lippard, S. J. (2003) New metal complexes as potential therapeutics. *Curr. Opin. Chem. Biol. 7*, 481−489.
(12) Ott, I., and Gust, R. (2007) Non platinum metal complexes as anti-cancer drugs. *Arch. Pharm. 340*, 117−126.
(13) Santini, C., Pellei, M., Gandin,V., Porchia, M., Tisato, F., and Marzano, C. (2013) Advances in copper complexes as anticancer agents. *Chem. Rev.* [Online early access] DOI: 10.1021/cr400135x. Published Online: Oct 8, 2013.
(14) Paterson, B. M., and Donnelly, P. S. (2011) Copper complexes of bis (thiosemicarbazones): From chemotherapeutics to diagnostic and therapeutic radiopharmaceuticals. *Chem. Soc. Rev. 40*, 3005−3018.
(15) Pelosi, G. (2010) Thiosemicarbazone metal complexes: From structure to activity. *Open Crystallogr. J. 3*, 16−28.

(16) Marzano, C., Pellei, M., Tisato, F., and Santini, C. (2009) Copper complexes as anticancer agents. *Anti-Cancer Agents Med. Chem. 9*, 185−211.
(17) Gupte, A., and Mumper, R. J. (2009) Elevated copper and oxidative stress in cancer cells as a target for cancer treatment. *Cancer Treat. Rev. 35*, 32−46.
(18) Lin, J., Haffner, M. C., Zhang, Y., Lee, B. H., NathanielBrennen, W., Britton, J., Kachhap, S. K., Shim, J. S., Liu, J. O., Nelson, W., Yegnasubramanian, S., and Carducci, M. A. (2011) Disulfiram is a DNA demethylating agent and inhibits prostate cancer cell growth. *Prostate 71*, 333−343.
(19) Schimmer, A. D., Jitkova, Y., Gronda, M., Wang, Z., Brandwein, J., Chen, C., Gupta, V., Schuh, A., Yee, K., Chen, J., Ackloo, S., Booth, T., Keays, S., and Minden, M. D. (2012) A phase I study of the metal ionophore clioquinol in patients with advanced hematologic malignancies. *Clin. Lymphoma, Myeloma Leuk. 12*, 330−336.
(20) Daniel, K. G., Gupta, P., Harbach, R. H., Guida, W. C., and Dou, Q. P. (2004) Organic copper complexes as a new class of proteasome inhibitors and apoptosis inducers in human cancer cells. *Biochem. Pharmacol. 67*, 1139−1151.
(21) Dearling, J. L. J., Lewis, J. L., Mullen, G. E. D., Welch, M. J., and Blower, P. J. (2002) Copper bis(thiosemicarbazone) complexes as hypoxia imaging agents: Structure-activity relationships. *J. Biol. Inorg. Chem. 7*, 249−259.
(22) Dilanyan, E. R., Ovsepyan, T. R., Arsenyan, F. G., Stepanyan, G. M., and Garibdzhanyan, B. T. (2008) Antitumour activity of substituted methylglyoxal bis-thiosemicarbazones and their copper(II) chelates. *Pharm. Chem. J. 42*, 504−506.
(23) Paterson, B. M., Karas, J. A., Scanlon, D. B., White, J. M., and Donnelly, P. S. (2010) Versatile new bis (thiosemicarbazone) bifunctional chelators: Synthesis, conjugation to bombesin (7-14)-NH_2, and copper-64 radiolabeling. *Inorg. Chem. 49*, 1884−1893.
(24) Donnelly, P. S., Liddell, J. R., Lim, S., Paterson, B. M., Cater, M. A., Savva, M. S., Mot, A. I., James, J. L., Trounce, I. A., White, A. R., and Crouch, P. J. (2012) An impaired mitochondrial electron transport chain increases retention of the hypoxia imaging agent diacetylbis(4-methylthiosemicarbazonato)copperII. *Proc. Natl. Acad. Sci. U.S.A. 109*, 47−52.
(25) Crouch, P. J., Hung, L. W., Adlard, P. A., Cortes, M., Lal, V., Filiz, G., Perez, K. A., Nurjono, M., Caragounis, A., Du, T., Laughton, K., Volitakis, I., Bush, A. I., Li, Q. X., Masters, C. L., Cappai, R., Cherny, R. A., Donnelly, P. S., White, A. R., and Barnham, K. J. (2009) Increasing Cu bioavailability inhibits Aβ oligomers and tau phosphorylation. *Proc. Natl. Acad. Sci. U.S.A. 106*, 381−386.
(26) Hung, L. W., Villemagne, V. L., Cheng, L., Sherratt, N. A., Ayton, S., White, A. R., Crouch, P. J., Lim, S., Leong, S. L., Wilkins, S., George, J., Roberts, B. R., Pham, C. L., Liu, X., Chiu, F. C., Shackleford, D. M., Powell, A. K., Masters, C. L., Bush, A. I., O'Keefe, G., Culvenor, J. G., Cappai, R., Cherny, R. A., Donnelly, P. S., Hill, A. F., Finkelstein, D. I., and Barnham, K. J. (2012) The hypoxia imaging agent CuII(atsm) is neuroprotective and improves motor and cognitive functions in multiple animal models of Parkinson's disease. *J. Exp. Med. 209*, 837−854.
(27) Belicchi-Ferrari, M., Bisceglie, F., Casoli, C., Durot, S., Morgenstern-Badarau, I., Pelosi, G., Pilotti, E., Pinelli, S., and Tarasconi, P. (2005) Copper(II) and cobalt(III) pyridoxal thiosemicarbazone complexes with nitroprusside as counterion: Syntheses, electronic properties, and antileukemic activity. *J. Med. Chem. 48*, 1671−1675.
(28) Joksović, M. D., Bogdanović, G., Kojić, V., Szécsényi, K. M., Leovac, V. M., Jakimov, D., Trifunović, S., Marković, V., and Joksović, L. (2010) Synthesis, cytotoxic activity, and thermal studies of novel *N*-[(1,3-diphenylpyrazol-4-yl)methyl] α-amino acids. *J. Heterocycl. Chem. 47*, 850−856.
(29) Bhat, S. S., Kumbhar, A. A., Heptullah, H., Khan, A. A., Gobre, V. V., Gejji, S. P., and Puranik, V. G. (2011) Synthesis, electronic structure, DNA and protein binding, DNA cleavage, and anticancer activity of fluorophore-labeled copper(II) complexes. *Inorg. Chem. 50*, 545−558.
(30) Jansen, B. A. J., Wielaard, P., Kalayda, G. V., Ferrari, M., Molenaar, C., Tanke, H. J., Brouwer, J., and Reedijk, J. (2004) Dinuclear platinum complexes with N, N′-bis(aminoalkyl)-1,4-diaminoanthraquinones as linking ligands. Part I. Synthesis, cytotoxicity, and cellular studies in A2780 human ovarian carcinoma cells. *J. Biol. Inorg. Chem. 9*, 403−413.
(31) Kalayda, G. V., Jansen, B. A. J., Molenaar, C., Wielaard, P., Tanke, H. J., and Reedijk, J. (2004) Dinuclear platinum complexes with N, N′-bis(aminoalkyl)-1,4-diaminoanthraquinones as linking ligands. Part II. Cellular processing in A2780 cisplatin-resistant human ovarian carcinoma cells: New insights into the mechanism of resistance. *J. Biol. Inorg. Chem. 9*, 414−422.
(32) Molenaar, C., Teuben, J. M., Heetebrij, R. J., Tanke, H. J., and Reedijk, J. (2000) New insights in the cellular response of platinum anticancer compounds, using fluorophore labeled platinum complexes and digital fluorescence microscopy. *J. Biol. Inorg. Chem. 5*, 655−665.
(33) New, E. J., Duan, R., Zhang, J. Z., and Hambley, T. W. (2009) Investigations using fluorescent ligands to monitor platinum(IV) reduction and platinum(II) reactions in cancer cells. *Dalton Trans.*, 3092−3101.
(34) Goswami, T. K., Gadadhar, S., Roy, M., Nethaji, M., Karande, A. A., and Chakravarty, A. R. (2012) Ferrocene-conjugated copper(II) complexes of L-methionine and phenanthroline bases: Synthesis, structure, and photocytotoxic activity. *Organometallics 31*, 3010−3021.
(35) Lim, S., Price, K. A., Chong, S. F., Paterson, B. M., Caragounis, A., Barnham, K. J., Crouch, P. J., Peach, J. M., Dilworth, J. R., White, A. R., and Donnelly, P. S. (2010) Copper and zinc bis-(thiosemicarbazonato) complexes with a fluorescent tag: Synthesis, radiolabelling with copper-64, cell uptake and fluorescence studies. *J. Biol. Inorg. Chem. 15*, 225−235.
(36) Frei, E., Luce, J. K., and Loo, T. L. (1971) Phase I and phototoxicity studies of Psuedourea. *Cancer Chemother. Rep., Part 1 55*, 91−96.
(37) Remers, W. A., Wunz, T. P., Dorr, R. T., Alberts, D. S., Tunget, C. L., Einspahr, J., and Milton, S. (1987) New antitumor agents containing the anthracene nucleus. *J. Med. Chem. 30*, 1313−1321.
(38) Kim, H. N., Lim, J., Lee, H. N., Ryu, J. W., Kim, M. J., Lee, J., Lee, D. U., Kim, Y., Kim, S. J., Lee, K., Lee, H. S., and Yoon, J. (2011) Unique X-ray sheet structure of 1,8-bis(imidazolium) anthracene and its application as a fluorescent probe for DNA and DNase. *Org. Lett. 13*, 1314−1317.
(39) Pittillo, R. F., and Woolley, C. (1969) Pseudourea, 2,2′-(9,10-anthrylenedimethylene) bis-(2-thio-, dihydrochloride) dihydrate: Microbiological assay and tissue distribution studies in mice. *Appl. Microbiol. 18*, 519−521.
(40) Wunz, T. P., Craven, M. T., Karol, M. D., Hill, G. C., and Remers, W. A. (1990) DNA binding by antitumor anthracene derivatives. *J. Med. Chem. 33*, 1549−1553.
(41) Iyengar, B. S., Dorr, R. T., Alberts, D. S., Solyom, A. M., Krutzsch, M., and Remers, W. A. (1997) 1,4-Disubstituted anthracene antitumor agents. *J. Med. Chem. 40*, 3734−3738.
(42) Modukuru, N. K., Snow, K. J., Perrin, B. S., Jr., Thota, J., and Kumar, C. V. (2005) Contributions of a long side chain to the binding affinity of an anthracene derivative to DNA. *J. Phys. Chem. B 109*, 11810−11818.
(43) Beckford, F. A., Shaloski, M., Jr., Leblanc, G., Thessing, J., Lewis-Alleyne, L. C., Holder, A. A., Li, L., and Seeram, N. P. (2009) Microwave synthesis of mixed ligand diimine−thiosemicarbazone complexes of ruthenium(II): Biophysical reactivity and cytotoxicity. *Dalton Trans.*, 10757−10764.
(44) Lakowicz, J. R. (2006) *Principles of Fluorescence Spectroscopy*, 3rd ed., Springer, New York.
(45) Chowdhury, N., Dasgupta, S., and Singh, N. D. P. (2012) Photoinduced DNA cleavage by anthracene based hydroxamic acids. *Bioorg. Med. Chem. Lett. 22*, 4668−4671.
(46) Sheldrick, G. M. (1997) SHELX-97 program for crystal structure solution and refinement, University of Göttingen, Göttingen, Germany.

(47) Wolfe, A., Shimer, G. H., and Meehan, T. (1987) Polycyclic aromatic hydrocarbons physically intercalate into duplex regions of denatured DNA. *Biochemistry 26*, 6392−6396.
(48) Quiming, N. S., Vergel, R. B., Nicolas, M. G., and Villanueva, J. A. (2005) Interaction of bovine serum albumin and metallothionein. *J. Health Sci. 51*, 8−15.
(49) Rajendiran, V., Karthik, R., Palaniandavar, M., Evans, H. S., Periasamay, V. S., Akbarsha, M. A., Srinag, B. S., and Krishnamurthy, H. (2007) Mixed-ligand copper(II)-phenolate complexes: Effect of coligand on enhanced DNA and protein binding, DNA cleavage, and anticancer activity. *Inorg. Chem. 46*, 8208−8228.
(50) Barve, A., Kumbhar, A., Bhat, M., Joshi, B., Butcher, R., Sonawane, U., and Joshi, R. (2009) Mixed-ligand copper(II) maltolate complexes: Synthesis, characterization, DNA binding and cleavage, and cytotoxicity. *Inorg. Chem. 48*, 9120−9132.
(51) Cowley, A. R., Dilworth, J. R., Donnelly, P. S., and White, J. M. (2006) Copper complexes of thiosemicarbazone−pyridylhydrazine (THYNIC) hybrid ligands: A new versatile potential bifunctional chelator for copper radiopharmaceuticals. *Inorg. Chem. 45*, 496−498.
(52) Fu, X. F., Yue, Y. F., Guo, R., Li, L. L., Sun, W., Fang, C. J., Xu, C. H., and Yan, C. H. (2009) An enhanced fluorescence in a tunable face-to-face π-π stacking assembly directed by the H-bonding. *CrystEngComm 11*, 2268−2271.
(53) Amatore, C., Pinson, J., and Saveant, J. M. (1982) Are anion radicals unable to undergo radical-radical dimerization? *J. Electroanal. Chem. 137*, 143−148.
(54) Carano, M., Cicogna, F., Houben, J. L., Ingrosso, G., Marchetti, F., Mottier, L., Paolucci, F., Pinzino, C., and Roffia, S. (2002) Synthesis of heteroleptic anthryl-substituted β-ketoenolates of rhodium(III) and iridium(III): Photophysical, electrochemical, and EPR study of the fluorophore-metal interaction. *Inorg. Chem. 41*, 3396−3409.
(55) Inker, L. A., and Bard, A. J. (1979) Electrochemistry in liquid sulfur dioxide. 1. Oxidation of thianthrene, phenothiazine, and 9,10-diphenylanthracene. *J. Am. Chem. Soc. 101*, 2316−2319.
(56) Dietrich, M., and Heinze, J. (1990) On the determination of redox potentials of highly reactive aromatic mono-and multications. *J. Am. Chem. Soc. 112*, 5142−5145.
(57) Xiao, Z., Donnelly, P. S., Zimmermann, M., and Wedd, A. G. (2008) Transfer of copper between bis(thiosemicarbazone) ligands and intracellular copper-binding proteins. Insights into mechanisms of copper uptake and hypoxia selectivity. *Inorg. Chem. 47*, 4338−4347.
(58) Sioda, R. E. (1968) Electrolytic oxidation of 9,10-diphenylanthracene and properties of its free radical cation and anion. *J. Phys. Chem. 72*, 2322−2330.
(59) Visco, R. E., and Chandross, E. A. (1964) Electroluminescence in solutions of aromatic hydrocarbons. *J. Am. Chem. Soc. 86*, 5350−5351.
(60) Given, P. H. (1958) Polarography of conjugated systems in dimethylformamide. *J. Chem. Soc.*, 2684−2687.
(61) Jamieson, E. R., and Lippard, S. J. (1999) Structure, recognition, and processing of cisplatin−DNA Adducts. *Chem. Rev. 99*, 2467−2498.
(62) Tysoe, S. A., Morgan, R. J., Baker, A. D., and Strekas, T. C. (1993) Spectroscopic investigation of differential binding modes of Δ- and Λ-Ru(bpy)$_2$(ppz)$^{2+}$ with calf thymus DNA. *J. Phys. Chem. 97*, 1707−1711.
(63) Kelly, J. M., Tossi, A. B., McConnell, D. J., and OhUigin, C. (1985) A study of the interactions of some polypyridyl ruthenium complexes with DNA using fluorescence spectroscopy, topoisomerisation and thermal denaturation. *Nucleic Acids Res. 13*, 6017−6034.
(64) Haworth, I. S., Elcock, A. H., Freemann, J., Rodger, A., and Richards, W. G. (1991) Sequence selective binding to the DNA major groove: Tris(1,10-phenanthroline)metal complexes binding to poly-(dG-dC) and poly(dA-dT). *J. Biomol. Struct. Dyn. 9*, 23−44.
(65) Waring, M. J. (1965) Complex formation between ethidium bromide and nucleic acids. *J. Mol. Biol. 13*, 269−282.
(66) Changzheng, I., Jigui, W., Liufang, W., Min, R., Naiyang, J., and Jie, G. (1999) Synthesis, characterization and antitumor activity of copper(II) complex with nicotinamido-4-bis(2-chloroethyl) amino-benzaldimine. *J. Inorg. Biochem. 73*, 195−202.
(67) Ramakrishnan, S., Rajendiran, V., Palaniandavar, M., Periasamy, V. S., Srinag, S., and Akbarsha, M. A. (2009) Induction of cell death by ternary copper(II) complexes of L-tyrosine and diimines: Role of coligands on DNA binding and cleavage and anticancer activity. *Inorg. Chem. 48*, 1309−1322.
(68) Shi, S., Liu, J., Li, J., Zheng, K. C., Tan, C. P., Chen, L. M., and Ji, L. N. (2005) Electronic effect of different positions of the $-NO_2$ group on the DNA-intercalator of chiral complexes $[Ru(bpy)_2L]^{2+}$ (L = *o*-npip, *m*-npip and *p*-npip). *Dalton Trans.*, 2038−2046.
(69) Gibellini, D., Vitone, F., Schiavone, P., Ponti, C., Placa, M. L., and Re, M. C. (2004) Quantitative detection of human immunodeficiency virus type 1 (HIV-1) proviral DNA in peripheral blood mononuclear cells by SYBR green real-time PCR technique. *J. Clin. Virol. 29*, 282−289.
(70) Ware, W. R. (1962) Oxygen quenching of fluorescence in solution: An experimental study of the diffusion process. *J. Phys. Chem. 66*, 455−458.
(71) Gao, C. Y., Qiao, X., Ma, Z. Y., Wang, Z. G., Lu, J., Tian, J. L., Xu, J. Y., and Yan, S. P. (2012) Synthesis, characterization, DNA binding and cleavage, BSA interaction and anticancer activity of dinuclear zinc complexes. *Dalton Trans. 41*, 12220−12232.
(72) Ross, D. P., and Subramanian, S. (1981) Thermodynamics of protein association reactions: Forces contributing to stability. *Biochemistry 20*, 3096−3102.
(73) Hu, Y. J., Liu, Y., Shen, X. S., Fanf, X. Y., and Qu, S. S. (2005) Studies on the interaction between 1-hexylcarbamoyl-5-fluorouracil and bovine serum albumin. *J. Mol. Struct. 738*, 143−147.
(74) Messori, L., Orioli, P., Vullo, D., Alessio, E., and Lengo, E. (2000) A spectroscopic study of the reaction of NAMI, a novel ruthenium(III) anti-neoplastic complex, with bovine serum albumin. *Eur. J. Biochem. 267*, 1206−1213.
(75) Shao, J., Zhou, B., Bernard, C., and Yen., Y. (2006) Ribonucleotide reductase inhibitors and future drug design. *Curr. Cancer Drug Targets 6*, 409−431.
(76) Thelander, L., and Reichard, P. (1979) Reduction of ribonucleotides. *Annu. Rev. Biochem. 48*, 133−158.
(77) Cory, J. G., and Sato, A. (1983) Regulation of ribonucleotide reductase activity in mammalian cells. *Mol. Cell. Biochem. 53*−*54*, 257−266.
(78) Nocentini, G. (1996) Ribonucleotide reductase inhibitors: New strategies for cancer chemotherapy. *Crit. Rev. Oncol. Hematol. 22*, 89−126.
(79) Cory, J. G. (1988) Ribonucleotide reductase as a chemotherapeutic target. *Adv. Enzyme Regul. 27*, 437−455.
(80) Lien, E. J. (1987) Ribonucleotide reductase inhibitors as anticancer and antiviral agents. *Prog. Drug Res. 31*, 101−126.
(81) Shao, J., Zhou, B., Di Bilio, A. J., Zhu, L., Wang, T., Qi, C., Shih, J., and Yen, Y. A (2006) Ferrous-triapine complex mediates formation of reactive oxygen species that inactivate human ribonucleotide reductase. *Mol. Cancer Ther. 5*, 586−592.
(82) Agrawal, K. C., and Sartorelli, A. C. (1978) The chemistry and biological activity of alpha-(N)-heterocyclic carboxaldehyde thiosemicarbazones. *Prog. Med. Chem. 15*, 321−356.
(83) Chaston, T. B., Lovejoy, D. B., Watts, R. N., and Richardson, D. R. (2003) Examination of the antiproliferative activity of iron chelators: Multiple cellular targets and the different mechanism of action of triapine compared with desferrioxamine and the potent pyridoxal isonicotinoyl hydrazone analogue 311. *Clin. Cancer Res. 9*, 402−414.
(84) Li, L., Wong, Y., Chen, T., Fan, C., and Zheng, W. (2012) Ruthenium complexes containing bis-benzimidazole derivatives as a new class of apoptosis inducers. *Dalton Trans. 41*, 1138−1141.
(85) Agarwal, M. K., Hastak, K., Jackson, M. W., Breit, S. N., Stark, G. R., and Agarwal, M. L. (2006) Macrophage inhibitory cytokine 1 mediates a p53-dependent protective arrest in S phase in response to starvation for DNA precursors. *Proc. Natl. Acad. Sci. U.S.A. 103*, 16278−16283.
(86) Demidenko, Z. N., Kaluruppalle, S., Hanko, C., Lim, C., Broude, E., and Blagosklonny, M. V. (2008) Mechanism of G1-like arrest by

low concentrations of paclitaxel: next cell cycle p53-dependent arrest with sub G1 DNA content mediated by prolonged mitosis. *Oncogene 27*, 4402−4410.
(87) Moll, U. M., and Concin, N. (2005) p53 in human cancer − somatic and inherited mutations and mutation-independent mechanisms. In *The p53 Tumor Suppressor Pathway and Cancer* (Zambetti, G. P., Ed.) p 115, Vol 2, Springer, New York.